ACS OMEGA

Open Access

http://pubs.acs.org/journal/acsodf

Article

Electrochemiluminescence Properties and Sensing Application of Zn(II)−Metal−Organic Frameworks Constructed by Mixed Ligands of Para Dicarboxylic Acids and 1,10-Phenanthroline

Fei Nie,*[,§] Ru Yu,[§] Lina Wang,[§] Liping Jiang, Qi Wu, Wenhua Xu,* and Xiaolong Fu*

Cite This: *ACS Omega* 2023, 8, 43463−43473

Read Online

ACCESS | Metrics & More | Article Recommendations | Supporting Information

ABSTRACT: Four metal−organic frameworks (MOFs) were designed and prepared through a mixed-ligand strategy by controlling the combination of various dicarboxylic acid ligands with invariant center metal and *o*-phenanthroline heterocyclic ligand. The regulatory effects of ligand electronic band and crystal structure on the electrochemiluminescence (ECL) characteristics of MOFs were verified by experimental results and density functional theory (DFT) calculations. The flexible chain structure of MOF-2 promotes electron transfer between MOF electroactive free radicals and the co-reactant, making it show outstanding ECL characteristics among all of the four MOFs with the luminescence quantum efficiency 8.37 times that of tris(bipyridine)-ruthenium(II) ($[Ru(bpy)_3]^{2+}$). Meanwhile, a new ECL mechanism for MOF luminescent crystal materials with reactive oxygen species in solvents as a co-reactant in the aqueous aerobic environment has been proposed. MOF-2 was selected to construct an ECL sensor for the determination of glucose in human urine samples. This study provides a useful idea for the development and design of new luminescent molecular crystal materials.

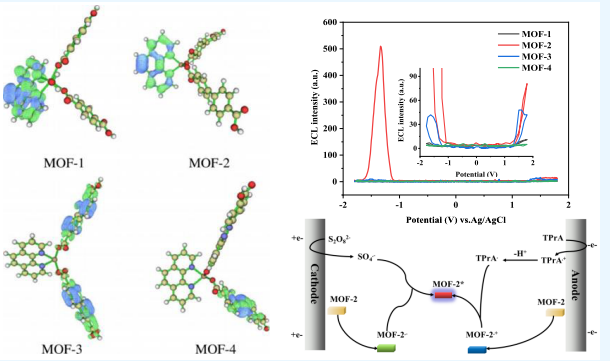

1. INTRODUCTION

Electrochemiluminescence (ECL) is a redox-induced process, in which luminophores are commanded by the application of an appropriate potential to generate electronically excited states at the electrodes and then relax and emit light.[1−3] In general, ECL emitters and co-reactants are the two key factors affecting the development of ECL. The development of new ECL emitters has been the focus of ECL research because of their important role in the conversion of electrical energy into radiant energy. The development of more efficient co-reactive reagents is also an important subject of ECL research because the co-reactants are irreplaceable to help produce higher ECL efficiency and better operability in most practical applications. In addition to three types of typical ECL materials, such as tris(bipyridine)-ruthenium(II) ($[Ru(bpy)_3]^{2+}$), luminol, and various quantum dots (QDs),[4] the development of various new ECL materials has attracted researchers.

Metal−organic frameworks (MOFs), also called porous coordination polymers (PCPs), are emerging porous and crystalline materials built from metal ions/clusters and organic linkers.[5,6] Owing to their intriguing topological structures, MOFs have versatile application prospects in many fields such as chemical sensing,[7] fluorescence,[8] supercapacitors,[9] gas sorption,[10] separation,[11] catalysis,[12] and so forth. In recent years, MOFs have also shown promising prospects in the synthesis of high-performance ECL materials. MOFs can be used to encapsulate different kinds of ECL materials[13−15] due to their ultrahigh specific surface area and functionable pores.[16] The excellent structural flexibility of MOFs[17] integrates luminescent clusters and co-reactant accelerators into the frame structure, effectively shortening the electron transfer path between them and improving the luminous efficiency of ECL luminescent bodies.[15] The metal-centric ions or their ligands in MOFs can also be directly used as co-reaction accelerators to further enhance the luminous signal.[18,19]

In the construction of the above ECL materials, MOFs are used as a carrier. In fact, MOFs with ECL properties can also be prepared by selecting suitable metal ions and ligands. The most common ECL MOFs are ruthenium-based complexes. In addition, some MOFs composed of lanthanide ions (Ln^{3+}) and d^{10} metal-based MOFs are also considered to have good ECL activity. In order to improve the electrochemical activity of MOFs, ligands with reduction−oxidization activity, such as bipyridine, tripyridine, and 1,10-phenanthrene, have also been introduced in the construction of MOFs. Such ligands can

Received: April 14, 2023
Accepted: August 9, 2023
Published: November 7, 2023

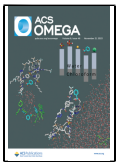

Scheme 1. Organic Carboxylates Used in This Work[a]

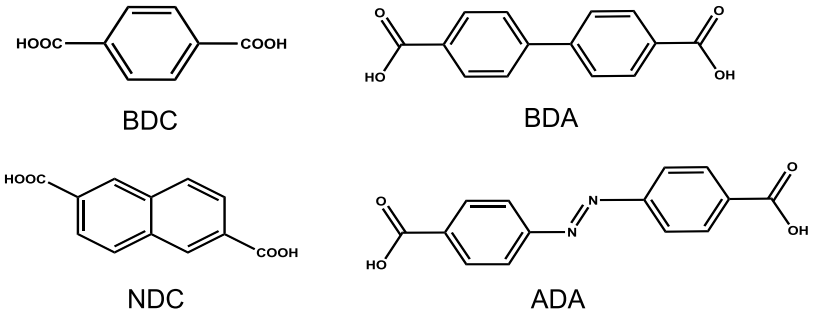

[a]BDC, benzene-1,4-dicarboxylic acid. BDA, biphenyl-4,4′-dicarboxylic acid. NDC, 2,6-naphthalenedicarboxylate. ADA, 4,4′-azodibenzoic acid.

enhance the electrochemical activity of MOFs and facilitate post-functionalization,[10] greatly improving the application prospect of MOF luminous materials in an aqueous phase.

As we all know, some key factors during the synthesis of MOF such as the type of metal ions or organic ligands,[20,21] reaction temperature,[22] pH of the system,[23] solvent,[24] etc. will restrict the frame structure of the prepared MOF material, thus affecting its performance. However, little attention has been paid to the influence of these factors on the electrochemical or luminescence properties of MOFs when studying their ECL properties, and useful conclusions can hardly be drawn to guide people to obtain effective ECL MOF materials. It is difficult to reach a satisfactory conclusion about whether MOFs with similar structure and composition have similar ECL properties.

In this paper, four zinc-based MOFs were synthesized with 1,10-phenanthroline (Phen) and four different para carboxylic acids including benzene-1,4-dicarboxylic acid (BDC), biphenyl-4,4′-dicarboxylic acid (BDA), 2,6-napthalenedicarboxylate (NDC), and 4,4′-azodibenzoic acid (ADA) using mixed-ligand strategy. Crystallographic studies showed that the four MOFs have a similar one-dimensional chain structure. Different kinds of para dicarboxylic acids regulated the twisting degree of MOF chain structure, resulting in Phen as the auxiliary ligand presenting different degrees of face-to-face stacking. Although all four MOFs composed of d^{10} metal zinc exhibit photoluminescence (PL) properties, we found that only MOF-2 composed of the BDA carboxylate ligand showed significant ECL at both cathode and anode without the addition of co-reactants, while the other three MOFs have weak or no ECL properties. Experiments showed that different organic ligands can regulate the electron band structure of MOFs, thus affecting the ECL efficiency of MOFs. This prediction is further supported by density functional theory (DFT) calculations. The commonly used cathodic and anodic ECL co-reactants of $K_2S_2O_8$ and tripropylamine (TPrA) could enhance the ECL signals of several MOFs, among which the ECL efficiency of MOF-2/$K_2S_2O_8$ system is the highest with an ECL efficiency of 837% when $[Ru(bpy)_3]^{2+}$ was taken as the reference (ECL efficiency is 100%).[25] Based on the principle that glucose oxidase (GOx) catalyzes glucose oxidation to produce hydrogen peroxide, which inhibits the ECL signal of the MOF-2/$K_2S_2O_8$ system, an ECL biosensor was constructed to the sensitive detection of glucose and has been successfully applied to the determination of glucose content in urine.

2. EXPERIMENTAL SECTION

2.1. Materials. All reagents and solvents were commercially available and used directly without any further purification. 1.10-Phenanthroline (Phen), zinc nitrate hexahydrate ($Zn(NO_3)_2{\cdot}6H_2O$), *N*,*N*-dimethylformamide (DMF), sodium phosphate monobasic dihydrate ($NaH_2PO_4{\cdot}2H_2O$), disodium hydrogen phosphate dodecahydrate ($Na_2HPO_4{\cdot}12H_2O$), and potassium persulfate ($K_2S_2O_8$) were obtained from Sinopharm Chemical Reagent Co., Ltd. (Shanghai). Benzene-1,4-dicarboxylic acid (BDC), biphenyl-4,4′-dicarboxylic acid (BDA), 2,6-napthalenedicarboxylate (NDC), and 4,4′-azodibenzoic acid (ADA) were all purchased from Aladdin. Phosphate buffer solution (PBS, 0.1 M, pH 7.4) was prepared by mixing stock solutions of NaH_2PO_4, Na_2HPO_4, and KCl. All chemicals were of analytical grade. The schematic representation of four different carboxylic acid ligands was shown in Scheme 1.

2.2. Apparatus. X-ray signal crystal diffraction patterns were measured by a Bruker SMART APEXCCD X-ray diffractometer with Mo Kα radiation (Bruker, Germany). Powder X-ray diffraction (PXRD) data were obtained on a Bruker D8-Advance X-ray powder diffractometer using Cu Kα radiation (Bruker, Germany) at 40 mA and 40 kV with 0.2 s per step, and the data were collected within the 2θ range of 5−50. The ultraviolet adsorption spectra were scanned from 200 to 450 nm on a UV-3310 ultraviolet−visible spectrophotometer (Shimadzu, Japan). Photoluminescence (PL) spectra were performed on an RF-5301PC fluorescence spectrophotometer (Shimadzu, Japan). Fourier transform infrared (FT-IR) spectra were recorded in the range from 4000 to 400 cm^{-1} on a Bruker EQUINOX-55 spectrophotometer (Bruker, Germany) using KBr pellets. The experimental measurements for cyclic voltammograms (CV) and ECL were recorded on MPI-E multifunctional EC and CL analytical system (Xi'an Remax Electronic Science & Technology Co. Ltd., Xi'an, China). A conventional three-electrode system was used for CV and ECL measurements with a glassy carbon electrode (GCE, 3 mm in diameter) used as the working electrode, a platinum wire as the counter electrode, and an Ag/AgCl (saturated KCl solution) electrode as the reference electrode, respectively. ECL spectra were obtained by a self-made ECL spectrum analyzer consisting of a CHI-660D electrochemical workstation and a Fluorolog-3 fluorescence spectrophotometer (Horiba JY) or with filters of various wavelengths from 400 to 760 nm. Electrochemical impedance spectroscopy (EIS) experiments were performed with a CHI-660E electrochemical workstation.

2.3. Preparation of Zinc-Based MOFs. *2.3.1. Synthesis of [Zn(BDC)(Phen)(OH)]$_n$ (MOF-1).* Briefly, a mixture of BDC

https://doi.org/10.1021/acsomega.3c02559
ACS Omega 2023, 8, 43463−43473

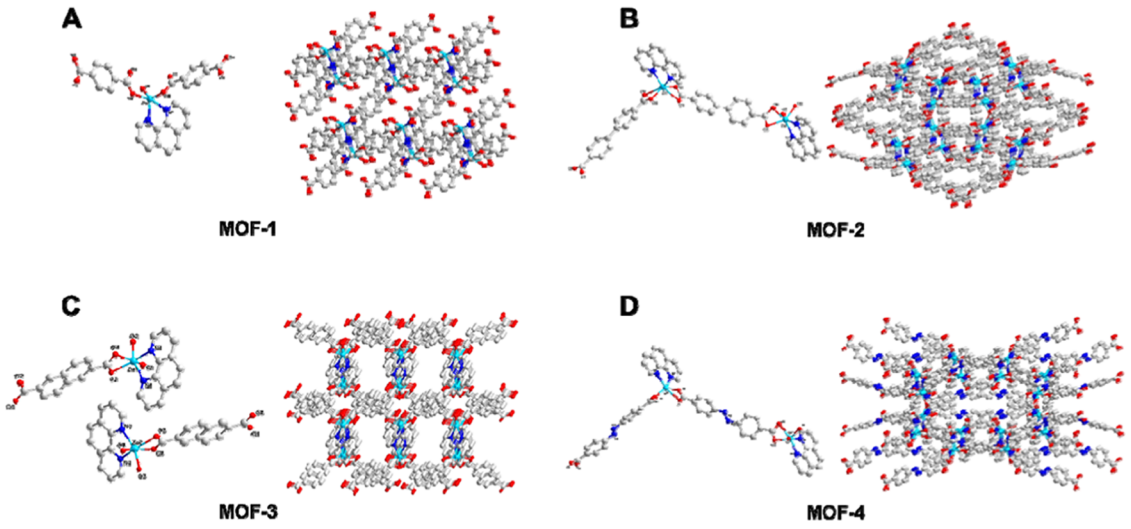

Figure 1. Crystal structures of (A) MOF-1, (B) MOF-2, (C) MOF-3, and (D) MOF-4.

(0.016 g, 0.1 mmol), Phen (0.019 g, 0.1 mmol), and $Zn(NO_3)_2{\cdot}6H_2O$ (0.030 g, 0.1 mmol) was stirred in the mixture of 3 mL of DMF, 3 mL of MeOH, and 3 mL of H_2O for 30 min at room temperature. The mixture was poured into a Teflon-lined autoclave (25 mL) and then heated at 120 °C for 72 h. White crystals of MOF-1 were collected by filtration, washed with DMF, and dried in air.

2.3.2. Synthesis of {[Zn(BDA)(Phen)]$_2$·DMF}$_n$ (MOF-2). A mixture of BDA (0.024 g, 0.1 mmol), Phen (0.019 g, 0.1 mmol), and $Zn(NO_3)_2{\cdot}6H_2O$ (0.030 g, 0.1 mmol) was stirred in the solvent of DMF and H_2O with a volume ratio of 7:3 for 30 min at room temperature. Then, it was poured into a Teflon-lined autoclave (25 mL). The autoclave was cooled slowly to room temperature after heating to 120 °C for 72 h. Pale yellow crystals of MOF-2 were collected by filtration, washed with DMF, and dried in the air.

2.3.3. Synthesis of {[Zn(NDC)(Phen)]·DMF}$_n$ (MOF-3). MOF-3 was obtained in a similar way as that for MOF-2, except that NDC (0.022 g, 0.1 mmol) was employed instead of BDA. The transparent rhombus crystals of MOF-3 were collected by filtration, washed with DMF, and dried in the air.

2.3.4. Synthesis of [Zn(ADA)(Phen)]$_n$ (MOF-4). MOF-4 was also synthesized in the same way as MOF-2, except that ADA (0.027 g, 0.1 mmol) was used instead of BDA. Reddish brown crystals of MOF-4 were collected by filtration, washed with DMF, and dried in the air.

2.3.5. Synthesis of the MOFs 1−4 Powder. Phen (0.1 mmol) and $Zn(NO_3)_2{\cdot}6H_2O$ (0.1 mmol) with different carboxylic acid ligands (0.1 mmol) were dissolved in 7 mL of DMF respectively and stirred in the air at 120 °C for 3 h. The powder was collected by centrifugation, washed with DMF, and dried in the air for the next experiments.

2.4. ECL Measurement. Prior to modification, the glassy carbon electrode was first polished with 0.3 and 0.05 mm alumina powder to obtain a mirror-like surface, followed by ultrasonic treatment with deionized water and ethanol respectively. Then, the GCE was allowed to dry at room temperature. Ten microliters of the MOF/H_2O dispersion liquid (1.0 mg/mL) was dropped on the GCE surface and then dried at room temperature. The CV and corresponding ECL measurements were recorded with a designated PMT in 0.1 M PBS (pH = 7.4) containing a 0.1 M $K_2S_2O_8$ solution. As a control, each component of MOF-2 including zinc ion, Phen and BDA was modified on GCE and their ECL signals were measured as previously described in the determination of MOF-2.

2.5. Construction of the Sensor. Five microliters of the MOF-2 suspension (1.0 mg/mL, prepared with 0.5% chitosan) was dropped onto the pretreated GCE and then dried in the air. Subsequently, 10 μL of the GOx solution (10 mg/mL, prepared with 0.1 M pH 7.4 PBS) was dropped on the electrode. During the fabrication of the biosensor, for each modification step, the electrode was washed with PBS to eliminate the nonspecific binding substances, and the obtained biosensor (GOx/chitosan-MOF-2/GCE) was stored at 4 °C for further use.

3. RESULTS AND DISCUSSION

3.1. Synthesis and Structural Determination of MOFs. The X-ray single-crystal structure assays indicate that all MOFs form a one-dimensional zigzag chain structure. MOF-1 crystallized in the triclinic crystal system with the P1 space group, which was a five-coordinate with two nitrogen atoms from the Phen ligand and two oxygen atoms from the carboxylate group of two different terephthalic acid and one oxygen atom from the coordinated water molecule (Figure 1A). MOF-2 crystallized in a monoclinic crystal system with the space group *C*2/*c*. For the two Zn(II) centers, Zn(1) is considered to be a kind of open metal site with five-coordinated two nitrogen atoms from the Phen ring and three oxygen atoms from two carboxylate groups of two different biphenyldicarboxylic acid molecules. It exhibited a distorted square-pyramidal geometry. Zn(2) is surrounded by two nitrogen atoms from the Phen ligand and four oxygen atoms from two carboxylate groups of two different biphenyldicarboxylic acid molecules in a distorted octahedral geometry. Figure 1B shows the face-to-face interaction between the Phen rings with the centroids of 3.418 and 3.584 Å.[26] MOF-3 crystallized in a monoclinic crystal system with the space group P2/c. The metal centers of Zn(1) and Zn(2) are chelated to two carboxylate groups of two NDC subunits, and the other two coordination sites on the Zn(II) centers are occupied by one Phen unit.[27] These chains align in parallel by the C−H···OCO action of the NDC, and these

https://doi.org/10.1021/acsomega.3c02559
ACS Omega 2023, 8, 43463−43473

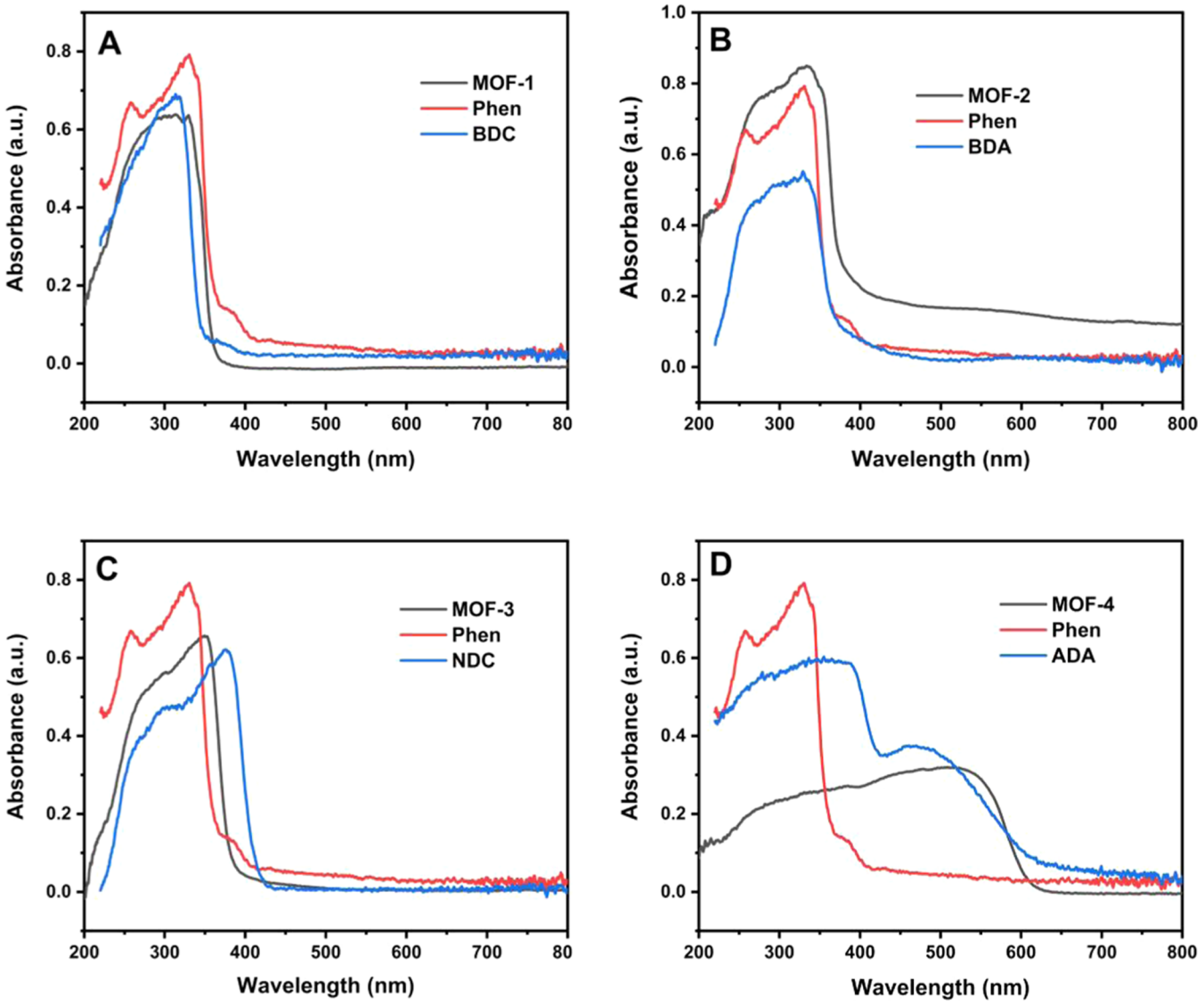

Figure 2. Solid-state UV−vis absorption spectra of (A) MOF-1 and the ligands, (B) MOF-2 and the ligands, (C) MOF-3 and the ligands, and (D) MOF-4 and the ligands.

interactions lead to the formation of two-dimensional corrugated plates in the crystal plane (Figure 1C). In Figure 1D, MOF-4 also crystallized in a monoclinic crystal system with the space group $C2/c$. Each Zn(II) center is hexacoordinated in a distorted octahedral geometry consisting of two nitrogen donors from one Phen ring and four oxygen atoms from two carboxylate groups of two different ADA ligands. The packing of the chains is dominated by $\pi-\pi$ interaction between Phen rings between the chains with a distance of 4.08 Å.[26] Table S1 shows the crystal data for the four MOFs. The PXRD patterns of all kinds of the four MOF materials are collected (Figure S1). The PXRD pattern of four MOFs can be readily compared with the simulated patterns from the single-crystal X-ray data. The positions of the main peaks from the as-prepared samples match well with the simulated pattern, thus demonstrating the high purity of the synthesized products. For the FT-IR, the C═N and carboxyl absorption peaks in the four MOFs showed different degrees of blue-shift compared with the Phen or the dicarboxylic acid ligands, indicating that Phen and deprotonated carboxyl ligands were coordinated with metal ions in four MOFs, respectively (Figure S2).

3.2. UV Absorption and Photoluminescence Performances. The luminescence properties of the d^{10} metal complex are usually determined by the ligands.[28,29] The solid-state UV−vis absorption spectra of the four MOFs and their ligands were collected and compared (Figure 2). The maximum absorption wavelength of MOF-1 and -2 are almost identical to the absorption peaks of Phen (258 and 329 nm). In contrast, MOF-3 and -4 show a wider absorption band, with their maximum absorption wavelengths closer to that of the carboxylate ligand. Especially for MOF-4, its absorption peak red-shifted by about 50 nm compared with that of ADA. Using the Kubelka−Munk function[30] to convert the reflectance into the equivalent absorption spectrum, the band gap energy E_g can be obtained directly from the $[F(R\infty)\cdot h\nu]^{1/2}$ curve (Figure S3), which are 3.39, 3.25, 3.26, and 2.00 eV for MOF-1−4, respectively. This indicates that the newly synthesized MOFs are all semiconductors with good electric conductivity. The experimental band gap order was reproduced by periodic

https://doi.org/10.1021/acsomega.3c02559
ACS Omega 2023, 8, 43463−43473

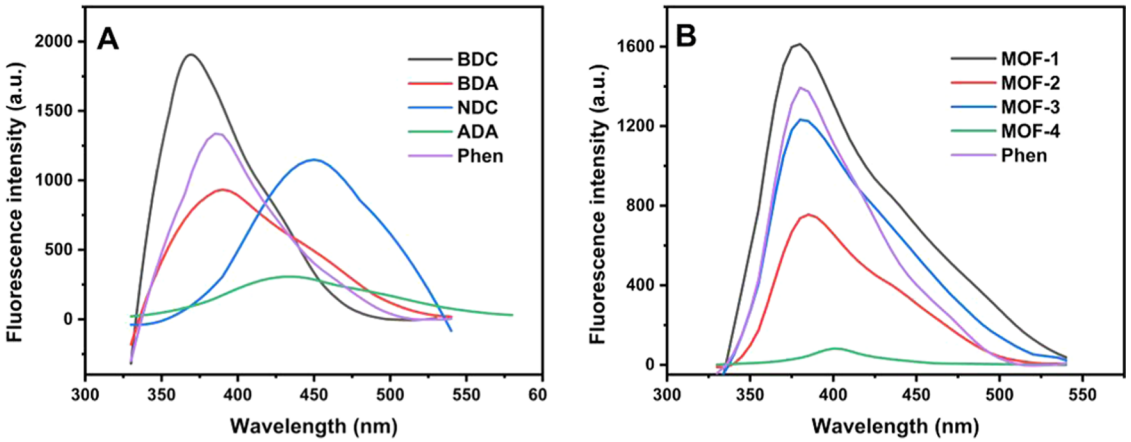

Figure 3. Solid-state fluorescence behaviors of (A) ligands and (B) MOF-1−4 and Phen (λ_{ex} = 320 nm).

density functional calculations (see the Supporting Information).

The solid-phase luminescence properties of four MOFs together with Phen and carboxylic acid ligands have been investigated at room temperature. The emission peaks of the ligand of Phen and carboxylic acid ligands of BDC, BDA, NDC, and ADA are at 385, 350, 390, 450, and 430 nm, respectively, which are ascribed to $\pi \rightarrow \pi^*$ or n $\rightarrow \pi^*$ transitions in these organic molecules (Figure 3A).[31] For the four types of MOFs, a single wide emission band was shown at 375, 380, 385, and 400 nm, respectively (Figure 3B), indicating that the maximum emission wavelength of MOF-1−3 was highly correlated with the Phen ligand after the ligand was complexed with Zn(II) ions, but its relative luminescence intensity was affected by the type of carboxylic acid ligand. Compared with other complexes, MOF-4 has the weakest fluorescence intensity and the emission wavelength does not coincide with that of Phen ligand and ADA carboxylic acid.

To reveal the characters of the excited states, time-dependent density functional calculations were performed (see the Supporting Information). The first singlet excited state (S_1) was the Phen local excitation for MOF-1 and MOF-2. By contrast, S_1 was the NDC or ADA local excitation for MOF-3 and MOF-4 (Figure 4). To account for the effect of crystal packing on the excited states, we take MOF-3 as an example, and two neighbor ligands were further added. The results are qualitatively similar to that without the two ligands. Note that compared with other low-lying excited states, the intensity of S_1 was usually rather low (Table S1). Relaxation of the S_1 states does not change their characteristics. Thus, the luminophores of MOF-1 and MOF-2 are the Phen ligand but are carboxylic acid ligands for MOF-3 and MOF-4. The computational findings complement the experimental data.

3.3. ECL Properties of the MOF−PBS System. The ECL measurement was first conducted with the MOF-modified GCE in an air-saturated PBS solution (0.10 M, pH = 7.4). The potential was cycled between −1.8 and 1.8 V using a CV mode at a scan rate of 100 mV/s (Figure 5A). When the potential was negatively scanned, two obvious reduction peaks appeared at −0.7 and −1.4 V. During the oxidation process, the current peak near 1.4 V occurred first and the oxidation current continued to increase until the potential reached 1.8 V. The electrochemical properties of MOF-2 were compared with those of its components, since it has the most prominent luminous property among the four MOFs (Figure S4A,C).

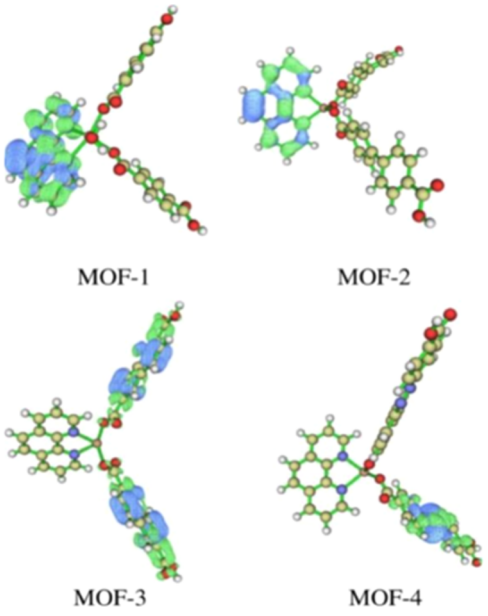

Figure 4. Hole and electron analysis of the first singlet excited state. The charge transfer is from the blue hole distribution to the green electron distribution. Isovalue = 0.002 au.

Thus, the two reduction peaks at −0.7 and −1.4 V should be associated with the reduction of dissolved oxygen and the injection of electrons into the lowest unoccupied molecular orbitals (LUMOs) of MOF to form the anionic radical ($MOF^{\bullet -}$). Here, MOF-4 is an exception because only one reduction peak was found in the −0.7 V cathode process, and no reduction peak attributed to MOF-4 itself was found. For the oxidation process, the oxidation peak at 1.4 V was considered to be the oxidation of MOF and then injected holes into the highest occupied molecular orbital (HOMO) of MOF to produce a cationic radical ($MOF^{\bullet +}$). Subsequently, the oxidation current continued to increase until the potential moved to 1.8 V, which may be due to the evolution of oxygen.[21] Further investigation of the effect of dissolved oxygen showed that the influence of oxygen concentration on the MOF cathodic ECL process is more significant than that on an anodic one (Figure S5).

Although only MOF-2 showed obvious ECL emission in both positive and negative potential regions when the scanning rate was 100 mV/s (Figure 5B), MOF-1 and MOF-3 exhibited

https://doi.org/10.1021/acsomega.3c02559
ACS Omega 2023, 8, 43463−43473

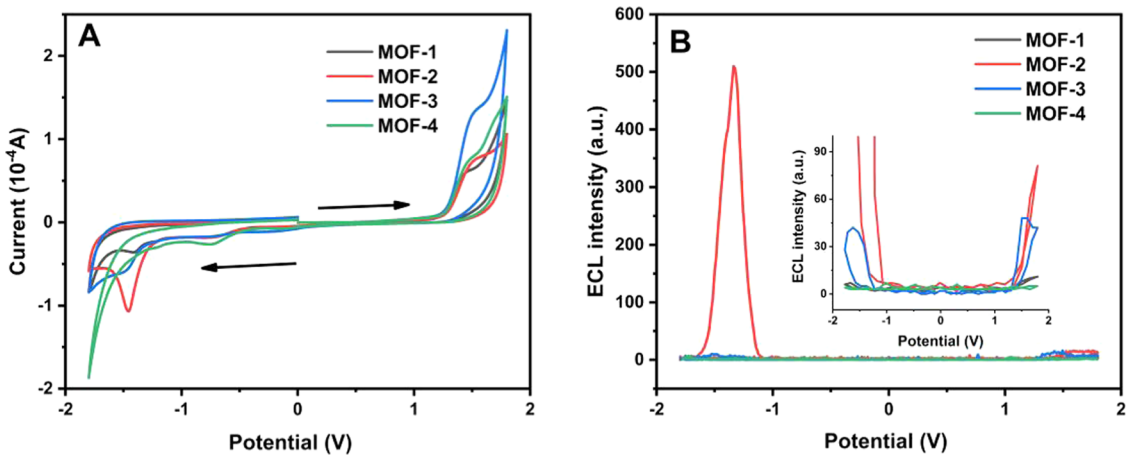

Figure 5. CV (A) and ECL response (B) of the MOF-1−4 powder at a scan rate of 0.1 V/s (the scan rate of the inset is 1.0 V/s).

similar ECL properties when the potential scanning speed increases to 1.0 V/s (inset Figure 5B) because the ECL signal is significantly enhanced with the increase of the scanning speed (Figure S6). It was noted that MOF-4 did not show significant ECL luminescence even with an increased scanning rate, which should be related to the weak photoluminescence intensity and the difficult electric reduction process of MOF-4. The stepping pulse (SP) approach was further employed to investigate the ECL behaviors of MOF-2 (Figure S7). MOF-2 can directly convert to the ECL excitons (MOF*) on the cathode or anode and emit ECL signals, different from other ECL substances that follow the annihilation mechanism. That means that it is not necessary to react the $MOF^{\bullet-}$ produced during the cathode electrochemical reduction with the $MOF^{\bullet+}$ produced by anode oxidation to obtain the exited state of MOF* for annihilation ECL. The ECL emission peak of MOF-2 is located at 460 nm with a red-shift of 80 nm compared to the fluorescence emission peak of MOF-2 at 380 nm (Figure S8), indicating that MOF-2, as an ECL luminous, may generate an ECL signal through a lower energy surface state transition mechanism.[23]

Based on the above experiments, we speculated the ECL mechanism of MOFs in the PBS solution, represented by the luminescence process of MOF-2. When the potential was scanned negatively, the dissolved oxygen in the PBS solution was first reduced to $O_2^{\bullet-}$ at −0.7 V (eq 1). The potential continued to shift negatively to −1.4 V, the component of Zn^{2+} and Phen in MOF-2 underwent an electrochemical reduction to generate $MOF\text{-}2^{\bullet-}$ (eq 2). The $MOF\text{-}2^{\bullet-}$ further reacted with the $O_2^{\bullet-}$ and produced an excited luminant (MOF-2*) (eq 3). When the excited MOF-2* returned to its ground state, the ECL signal was emitted (eq 4). The cathode luminescence process is as follows:

$$O_2 + e \rightarrow O_2^{\bullet-} \quad (1)$$

$$MOF\text{-}2 + e \rightarrow MOF\text{-}2^{\bullet-} \quad (2)$$

$$MOF\text{-}2^{\bullet-} + O_2^{\bullet-} \rightarrow MOF\text{-}2^{*} + O_2^{2-} \quad (3)$$

$$MOF\text{-}2^{*} \rightarrow MOF\text{-}2 + h\nu \quad (4)$$

During the electrochemical oxidation process of the anode, BDA in MOF-2 lost electrons to generate cationic radical $MOF\text{-}2^{\bullet+}$ (eq 5) when the potential was scanned forward to about 1.4 V. As the potential continued to move positively, the oxidation of water occurred and the hydroxyl radicals ($OH^{\bullet}$) generated (eq 6). The MOF-2 reacted with $OH^{\bullet}$ and was transferred into $MOF\text{-}2^{\bullet-}$ (eq 7). $MOF\text{-}2^{\bullet+}$ reacted with $MOF\text{-}2^{\bullet-}$ and generated an excited luminant (MOF-2*) (eq 8). The ECL signal was released when it returned to the ground state (eq 9). The anode luminescence process is as follows:

$$MOF\text{-}2 - e \rightarrow MOF\text{-}2^{\bullet+} \quad (5)$$

$$H_2O - e \rightarrow OH^{\bullet} + H^{+} \quad (6)$$

$$MOF\text{-}2 + OH^{\bullet} \rightarrow MOF\text{-}2^{\bullet-} + O_2 \quad (7)$$

$$MOF\text{-}2^{\bullet+} + MOF\text{-}2^{\bullet-} \rightarrow MOF\text{-}2^{*} \quad (8)$$

$$MOF\text{-}2^{*} \rightarrow MOF\text{-}2 + h\nu \quad (9)$$

Based on this mechanism, when the potential is scanned in the range of −1.8 to +1.8 V, the accumulation of $MOF\text{-}2^{\bullet-}$ during the electrochemical reduction process will promote the anode ECL while O_2 produced by anode ECL emission will continue to be used as a co-reactant promoting the cathodic ECL. Therefore, the ECL process of MOF-2 does not require additional co-reactant and the ECL intensity is considerable.

In order to further answer the question that the luminescence intensity of the four kinds of MOF is significantly different, we compared the electron density distribution of the four MOFs. As speculated above, the oxidized or reduced radical species of MOFs were involved in ECL processes. The electron spin density distributions of the cations resemble that of the HOMO of the neutral ones, so do the spin densities of the anions and the LUMO of the neutral MOFs (Figure S9). MOF-2 and MOF-3 have similar electron and hole localizations. The excess electrons of $[MOF\text{-}2]^{-}$/$[MOF\text{-}3]^{-}$ are localized on the Phen ligand, while the holes of $[MOF\text{-}2]^{+}$/$[MOF\text{-}3]^{+}$ are localized on the carboxylic acid ligands. By contrast, the excess electrons and holes of the MOF-1 and MOF-4 radicals are localized on the Phen or ADA carboxylate ligand. This further verified that it is difficult for the Phen ligand to be the electroreduction site in MOF-4 and for the carboxylic acid to be the oxidation site of MOF-1. It is also explained that it is difficult for MOF-1 and MOF-4 to generate very strong luminescence signals through the mechanism of mutual enhancement of cathode and anode luminescence. For MOF-2 and MOF-3, we noticed that the metal Zn in MOF-2 formed open metal sites due to incomplete

https://doi.org/10.1021/acsomega.3c02559
ACS Omega 2023, 8, 43463−43473

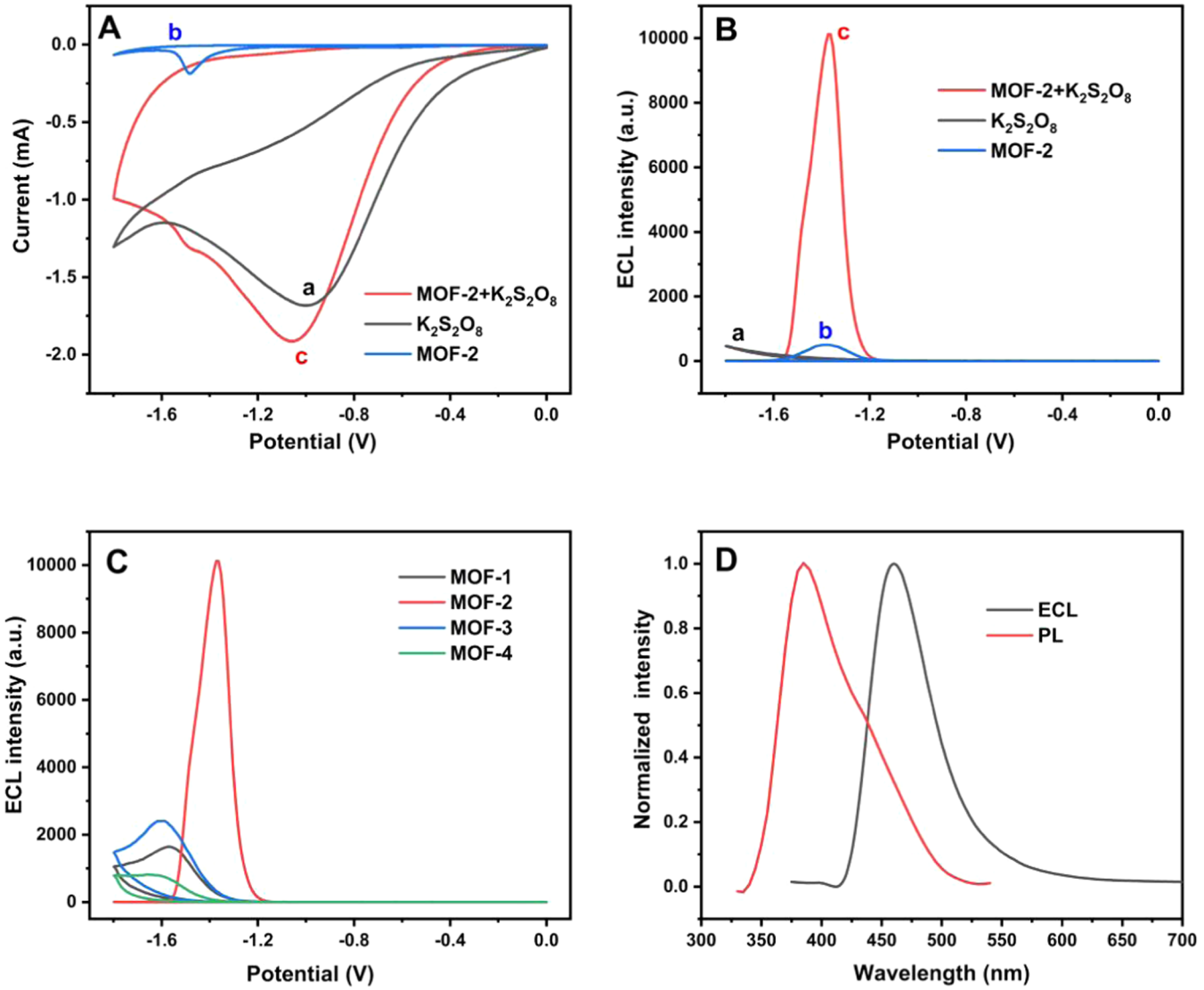

Figure 6. Cathodic (A) CV and (B) ECL of MOF-2/GCE (b, c) and bare GCE (a) in 0.1 M PBS solution without (b) and with (a, c) 0.1 M $K_2S_2O_8$. (C) ECL response of MOF-1−4 in a 0.1 M $K_2S_2O_8$ solution. (D) ECL spectrum and fluorescence spectrum of MOF-2 in a 0.1 M $K_2S_2O_8$ solution (λ_{ex} = 320 nm).

coordination,[32] which effectively improved the oxygen adsorption level (Figure S10). In addition, the increased flexibility of carboxylic acid ligands from NDC to BDA changed the crystal structure of MOFs from parallel chains to double helices (Figure S11). It is precisely because of the flexible helical chain structure of MOF-2 that the free radical MOF-2$^{\bullet-}$ formed at the Phen electroreduction site is close to the oxygen free radical, which greatly improves the probability of free radical reaction and greatly promotes the ECL signal of MOF-2.

3.5. ECL Properties of MOFs/Co-reactant System. In a cathodic ECL system, two obvious reduction peaks were produced when $K_2S_2O_8$ was added into the PBS solution, in which the co-reactant $S_2O_8^{2-}$ could be electrochemically reduced to a strong oxidizing intermediate ($SO_4^{\bullet-}$) at −1.0 V[24] and MOF-2 converted to MOF-2$^{\bullet-}$ by single electron reduction at −1.4 V (Figure 6A). An intensive ECL signal was observed with an onset potential around −1.0 V and maximum emission around −1.34 V (Figure 6B), which was consistent with the ECL of MOF-2 in PBS. It must be emphasized that the ECL signal of MOF-2 is too strong to be compared with the ECL signal without the use of a co-reactant under the same instrumental conditions by using the usual concentration of $K_2S_2O_8$ (0.1 M) as a co-reactant. Thus, the cathodic ECL signal of MOF-2 with only 0.002 M $K_2S_2O_8$ was compared with that of 50 times the amount of $K_2S_2O_8$ (0.1 M) on the bare GCE, and a 22-fold enhancement of the signal was observed. The ECL signal of the other three MOFs was also compared with that of MOF-2. The ECL signal of all MOFs was enhanced after the addition of co-reactant except for MOF-4, but the ECL signal of MOF-2 is always the strongest compared with the other three MOFs, although the concentration of the $K_2S_2O_8$ co-reactant was 50 times that of MOF-2 (Figure 6C). The ECL spectrum in the presence of the $K_2S_2O_8$ co-reactant is basically consistent with the ECL spectrum of MOF-2 in PBS, and the red-shift occurred compared with the PL of MOF-2 (Figure 6D). Therefore, the cathode ECL emission should be still generated by the MOF-2* in the presence of $K_2S_2O_8$, which acted as a co-reaction reagent and further amplified the ECL signal of MOF-2. Using

https://doi.org/10.1021/acsomega.3c02559
ACS Omega 2023, 8, 43463−43473

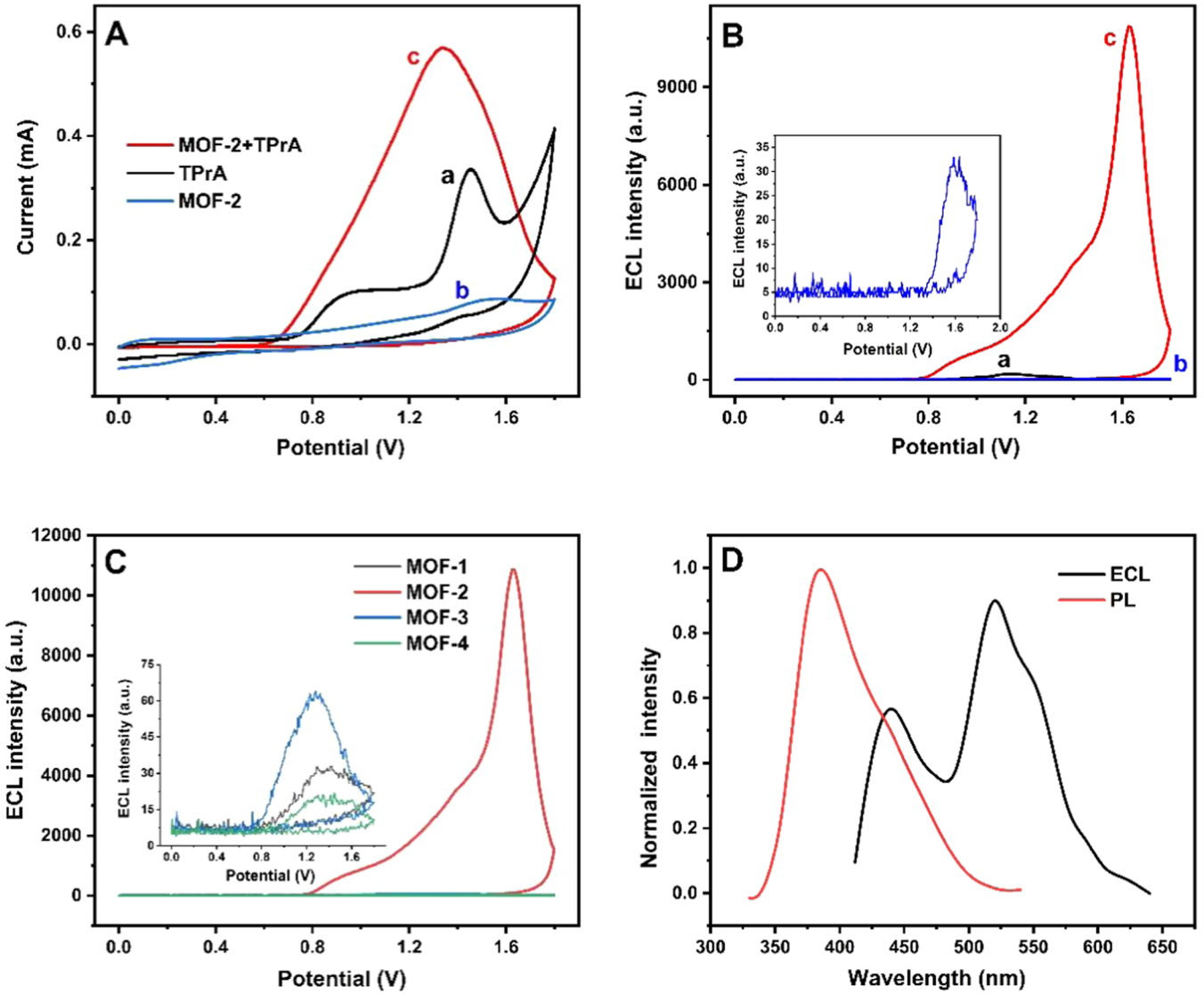

Figure 7. Anodic (A) CV and (B) ECL of MOF-2/GCE (b, c) and bare GCE (a) in 0.1 M PBS solution without (b) and with (a, c) 10 mM TPrA. (C) ECL response of MOF-1−4 in a 0.1 M PBS solution with 10 mM TPrA. (D) ECL spectrum and fluorescence spectrum of MOF-2 in 0.1 M PBS solution with 10 mM TPrA (λ_{ex} = 320 nm).

the routing $Ru(bpy)_3^{2+}/K_2S_2O_8$ ECL system as the reference (ECL quantum yield is defined as 100%)[33] and the ECL efficiency of MOF-2 was determined to be 837% (Figure S12).

Taking MOF-2 as an example, $K_2S_2O_8$ enhances the MOF ECL by the following mechanism. $S_2O_8^{2-}$ was electrochemically reduced to radical intermediate ($SO_4^{\bullet-}$) around −0.8 V (eq 10), which injected holes into the highest occupied molecular orbital (HOMO) of MOFs to produce a cationic radical (MOF-$2^{\bullet+}$) (eq 11). When the negative scanning potential reached −1.3 V, MOF-2 reduced to the MOF-2 anion radicals (MOF-$2^{\bullet-}$) on the electrode (eq 12), which reacted with $SO_4^{\bullet-}$ or MOF-$2^{\bullet+}$ and formed the exited state of luminant (MOF-2*) (eqs 13 and 14). Finally, MOF-2* returned to the ground state and emitted light (eq 15).

$$S_2O_8^{2-} + e \rightarrow SO_4^{\bullet-} + SO_4^{2-} \quad (10)$$

$$SO_4^{\bullet-} + \text{MOF-2} \rightarrow \text{MOF-2}^{\bullet+} + SO_4^{2-} \quad (11)$$

$$\text{MOF-2} + e \rightarrow \text{MOF-2}^{\bullet-} \quad (12)$$

$$\text{MOF-2}^{\bullet-} + SO_4^{\bullet-} \rightarrow \text{MOF-2}^{*} + SO_4^{2-} \quad (13)$$

$$\text{MOF-2}^{\bullet-} + \text{MOF-2}^{\bullet+} \rightarrow \text{MOF-2}^{*} \quad (14)$$

$$\text{MOF-2}^{*} \rightarrow \text{MOF-2} + h\nu \quad (15)$$

Similarly, enhanced oxidation current at 1.34 V (Figure 7A) and strong anodic ECL signal with an onset potential around +0.8 V and maximum emission around +1.5 V on the MOF-2-modified electrode (Figure 7B) was observed using TPrA as the anodic co-reactant reagent. Compared with the other MOFs, the anodic ECL intensity of MOF-2 is still the strongest, while only MOF-4 can hardly be enhanced by the TPrA co-reactant reagent (Figure 7C). The ECL emission peak of the MOF-2/TPrA system is 440 nm, which is not much different from the ECL emission peak of MOF-2 in PBS (460 nm), so the ECL of the MOF-2/TPrA system is still caused by MOF-2* (Figure 7D).

The ECL process of MOF-2 with TPrA as an anodic co-reactant is speculated as follows. TPrA could be electrochemically oxidized to TPrA$^{\bullet+}$ (eq 16), and it underwent

https://doi.org/10.1021/acsomega.3c02559
ACS Omega 2023, 8, 43463−43473

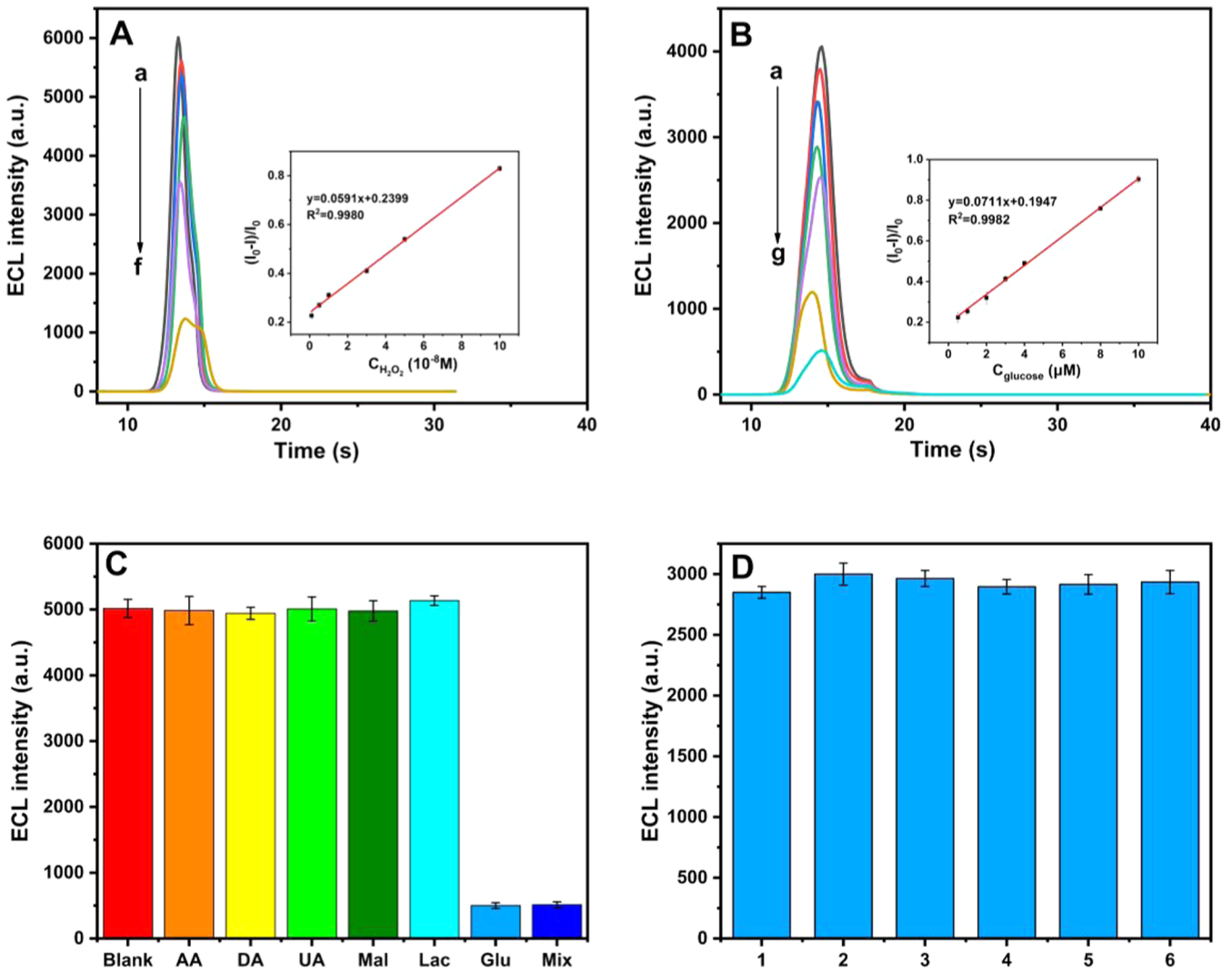

Figure 8. (A) ECL responses of the MOF-2/$K_2S_2O_8$ system for different concentrations of H_2O_2 [0.1, 0.5, 1.0, 3.0, 5.0, and 10.0 × 10^{-8} M (from a to f)]. (B) ECL responses of the MOF-2/$K_2S_2O_8$ system for different concentrations of glucose [0.5, 1.0, 2.0, 3.0, 4.0, 8.0, and 10.0 nM (from a to g)]. Inset shows the linear calibration curve. (C) ECL intensity for 2.0 μM Glu and 10 μM AA, DA, UA, Mal, and Lac. (D) Reproducibility of the sensor with 3.0 μM Glu using six modified electrodes in the same condition.

deprotonation to produce $TPrA^{\bullet}$ (eq 17).[34] As the potential shifted to more positive, MOF-2 could be electrochemically oxidized to MOF-$2^{\bullet+}$ (eq 18) and reacted with $TPrA^{\bullet}$ to generate MOF-2* (eq 19), which emitted light finally (eq 20).

$$TPrA - e \rightarrow TPrA^{\bullet+} \quad (16)$$

$$TPrA^{\bullet+} \rightarrow TPrA^{\bullet} + H^{+} \quad (17)$$

$$MOF\text{-}2 - e \rightarrow MOF\text{-}2^{\bullet+} \quad (18)$$

$$TPrA^{\bullet} + MOF\text{-}2^{\bullet+} \rightarrow MOF\text{-}2^{*} \quad (19)$$

$$MOF\text{-}2^{*} \rightarrow MOF\text{-}2 + h\nu \quad (20)$$

3.7. Determination of Glucose. The MOF-2/$K_2S_2O_8$ ECL system is used as a probe for practical analytical applications. Hydrogen peroxide was found to significantly inhibit the ECL signal in the MOF-2/$K_2S_2O_8$ system. Under the optimal experimental conditions (Figure S13), the ECL inhibition rate of the MOF-2/$K_2S_2O_8$ system was linear to the H_2O_2 concentration in the range of 10^{-9}–10^{-7} M, and the detection limit was 3.3 × 10^{-10} M (Figure 8A). Based on the inhibitory effect of H_2O_2 on the ECL signal of the MOF-2/$K_2S_2O_8$ system and the principle of glucose oxidase (GOx) catalytic oxidation of glucose, a glucose detection ECL sensor was constructed. Electrochemical impedance spectroscopy (EIS) was used to verify the various sensor preparation steps (Figure S14). Glucose was measured by an ECL sensor under the optimized experimental conditions and the inhibitory efficiency of ECL was linear with glucose concentration from 0.5 to 10 μM with the detection limit of 0.2 μM (S/N = 3) (Figure 8B). The ECL signal was not significantly different from that of the blank solution when the same concentrations of AA, Mal, Lac, DA, and UA (10 μM) were added to the PBS solution, respectively. The ECL signal of the mixture made of all these interfering substances with 2.0 μM glucose was basically consistent with that obtained using glucose alone (Figure 8C). Six ECL biosensors were prepared by the same procedure and used for the measurement of glucose with the same concentration (3.0 μM). The ECL intensity did not change significantly and the relative standard deviation (RSD) of the ECL signal was 1.8%, indicating that the sensor had good reproducibility (Figure 8D). The urine of two healthy people was collected as samples, and the content of glucose

https://doi.org/10.1021/acsomega.3c02559
ACS Omega 2023, 8, 43463−43473

was measured after these urine samples were diluted 1000 times with PBS solution and 0.1 M $K_2S_2O_8$ was added. Table 1

Table 1. Determination of Glucose in Human Urine Samples (n = 3)

sample	ECL method (μM)	amount added (μM)	amount found (μM)	recovery (%)	RSD (%)
1	0.58	2.00	2.47	96	2.8
	0.60	4.00	4.72	103	1.9
	0.62	8.00	8.75	102	3.4
2	0.94	2.00	2.81	96	1.6
	1.2	4.00	5.24	101	2.5
	1.1	8.00	8.86	97	3.7

shows the results of measuring glucose and spiked recovery in urine samples with the prepared sensor, indicating that the proposed ECL sensor can be used for glucose analysis in actual samples.

4. CONCLUSIONS

In summary, four zinc-based MOFs were designed and synthesized by a mixed-ligand strategy via a simple solvothermal method with different dicarboxylic acid ligands and Phen. Additionally, the cathodic and anodic ECL properties of the four zinc-based MOFs in PBS solution and with co-reactant were studied and compared, respectively. Among them, MOF-2 with the BDA carboxylic acid ligand has a strong ECL efficiency due to its open metal sites and the flexible structure of carboxylate ligands. Taking MOF-2 as an example, the ECL mechanism of MOF involving dissolved oxygen in aqueous solution was proposed. These MOFs can be used to design excellent ECL materials for practical application.

■ ASSOCIATED CONTENT

Supporting Information

The Supporting Information is available free of charge at https://pubs.acs.org/doi/10.1021/acsomega.3c02559.

Computational details of the DFT calculation, crystal data and X-ray experimental data for the four MOFs, excited states of the four MOFs, PXRD images of the four MOFs, FT-IR spectra of the four MOFs, band gap energy of the four MOFs, CV and ECL of MOF-2/GCE and its ligands, effect of dissolved oxygen on CV and ECL of MOF-2, effect of the scanning rates on the ECL of MOF-2/GCE, ECL transients of MOF-2/GCE by repetitively pulsing the potential, ECL and FL spectra of MOF-2, the HOMO and LUMO of the four MOFs, and spin densities of the MOF cations and anions, XPS spectra of O 1s on the surfaces of MOF-3 and MOF-2, the extended structures of MOF-2 and MOF-3, the comparison of the ECL signals of MOF-2 and $Ru(bpy)_3^{2+}$ in the PBS solution containing 0.1 M $K_2S_2O_8$, optimization of experimental conditions, and EIS characterization of the biosensor (PDF)

■ AUTHOR INFORMATION

Corresponding Authors

Fei Nie − *Key Laboratory of Synthetic and Natural Functional Molecule Chemistry (Ministry of Education), College of Chemistry & Materials Science, Northwest University, Xi'an 710069, P. R. China*; orcid.org/0000-0002-8680-9702; Email: niefei@nwu.edu.cn

Wenhua Xu − *Key Laboratory of Synthetic and Natural Functional Molecule Chemistry (Ministry of Education), College of Chemistry & Materials Science, Northwest University, Xi'an 710069, P. R. China*; Email: xuwenhua_qf@126.com

Xiaolong Fu − *Xi'an Modern Chemistry Research Institute, Xi'an 710062, P. R. China*; Email: fuxiaolong204@163.com

Authors

Ru Yu − *Key Laboratory of Synthetic and Natural Functional Molecule Chemistry (Ministry of Education), College of Chemistry & Materials Science, Northwest University, Xi'an 710069, P. R. China*

Lina Wang − *Key Laboratory of Synthetic and Natural Functional Molecule Chemistry (Ministry of Education), College of Chemistry & Materials Science, Northwest University, Xi'an 710069, P. R. China*

Liping Jiang − *Xi'an Modern Chemistry Research Institute, Xi'an 710062, P. R. China*

Qi Wu − *Key Laboratory of Synthetic and Natural Functional Molecule Chemistry (Ministry of Education), College of Chemistry & Materials Science, Northwest University, Xi'an 710069, P. R. China*

Complete contact information is available at: https://pubs.acs.org/10.1021/acsomega.3c02559

Author Contributions

§F.N., R.Y., and L.W. contributed equally to this work and should be considered co-first authors.

Notes

The authors declare no competing financial interest.

■ ACKNOWLEDGMENTS

The authors are grateful for the financial support from the Shaanxi Science and Technology Department (2022GY-384, 2022JBGS2-07, 2021LLRH-05-21, and S2022-YD-QFY-0107) and the Open Foundation of Key Laboratory of Synthetic and Natural Functional Molecular Chemistry of Ministry of Education (KLSNFM2020001).

■ REFERENCES

(1) Tokel, N. E.; Bard, A. J. Electrogenerated chemiluminescence. IX. Electrochemistry and emission from systems containing tris (2, 2′-bipyridine) ruthenium (II) dichloride. *J. Am. Chem. Soc.* **1972**, *94*, 2862−2863.

(2) Zhao, Y. R.; Yu, J.; Xu, G. B.; Sojic, N. O.; Loget, G. R. E. Photoinduced Electrochemiluminescence at Silicon Electrodes in Water. *J. Am. Chem. Soc.* **2019**, *141*, 13013−13016.

(3) Wu, Y. X.; Han, Z. G.; Wei, L. P.; Sun, H. S.; Wang, T. Y.; Chen, J.; Zhang, R. Z.; Lu, X. Q. Depolymerization-Induced Electrochemiluminescence of Insoluble Porphyrin in Aqueous Phase. *Anal. Chem.* **2020**, *92*, 5464−5472.

(4) Guo, W.; Ding, H.; Gu, C.; Liu, Y.; Jiang, X.; Su, B.; Shao, Y. Potential-resolved multicolor electrochemiluminescence for multiplex immunoassay in a single sample. *J. Am. Chem. Soc.* **2018**, *140*, 15904−15915.

(5) Shah, M. S.; Tsapatsis, M.; Siepmann, J. I. Hydrogen Sulfide Capture: From Absorption in Polar Liquids to Oxide, Zeolite, and Metal-Organic Framework Adsorbents and Membranes. *Chem. Rev.* **2017**, *117*, 9755−9803.

(6) Pan, Y.; Liu, W.; Liu, D.; Ding, Q.; Liu, J.; Xu, H.; Trivedi, M.; Kumar, A. A 3D metal-organic framework with isophthalic acid linker for photocatalytic properties. *Inorg. Chem. Commun.* **2019**, *100*, 92−96.
(7) Yan, B. Luminescence response mode and chemical sensing mechanism for lanthanide-functionalized metal-organic framework hybrids. *Inorg. Chem. Front.* **2021**, *8*, 201−233.
(8) Yao, S. L.; Liu, S. J.; Tian, X. M.; Zheng, T. F.; Cao, C.; Niu, C. Y.; Chen, Y. Q.; Chen, J. L.; Huang, H. P.; Wen, H. R. A Zn-II-Based Metal-Organic Framework with a Rare tcj Topology as a Turn-On Fluorescent Sensor for Acetylacetone. *Inorg. Chem.* **2019**, *58*, 3578−3581.
(9) Gao, S. W.; Sui, Y. W.; Wei, F. X.; Qi, J. Q.; Meng, Q. K.; Ren, Y. J.; He, Y. Z. Dandelion-like nickel/cobalt metal-organic framework based electrode materials for high performance supercapacitors. *J. Colloid Interface Sci.* **2018**, *531*, 83−90.
(10) Zhao, Y.; Wang, L.; Fan, N. N.; Han, M. L.; Yang, G. P.; Ma, L. F. Porous Zn(II)-Based Metal-Organic Frameworks Decorated with Carboxylate Groups Exhibiting High Gas Adsorption and Separation of Organic Dyes. *Cryst. Growth Des.* **2018**, *18*, 7114−7121.
(11) Fan, W. D.; Wang, X.; Zhang, X. R.; Liu, X. P.; Wang, Y. T.; Kang, Z. X.; Dai, F. N.; Xu, B.; Wang, R. M.; Sun, D. F. Fine-Tuning the Pore Environment of the Microporous Cu-MOF for High Propylene Storage and Efficient Separation of Light Hydrocarbons. *ACS Cent. Sci.* **2019**, *5*, 1261−1268.
(12) Hou, C. C.; Wang, H. F.; Li, C. X.; Xu, Q. From metal-organic frameworks to single/dual-atom and cluster metal catalysts for energy applications. *Energy Environ. Sci.* **2020**, *13*, 1658−1693.
(13) Yang, X.; Yu, Y. Q.; Peng, L. Z.; Lei, Y. M.; Chai, Y. Q.; Yuan, R.; Zhuo, Y. Strong Electrochemiluminescence from MOF Accelerator Enriched Quantum Dots for Enhanced Sensing of Trace cTnI. *Anal. Chem.* **2018**, *90*, 3995−4002.
(14) Wang, S. S.; Wang, M. M.; Li, C. P.; Li, H. J.; Ge, C. H.; Zhang, X. D.; Jin, Y. D. A highly sensitive and stable electrochemiluminescence immunosensor for alpha-fetoprotein detection based on luminol-AgNPs@Co/Ni-MOF nanosheet microflowers. *Sens. Actuators, B* **2020**, *311*, No. 127919.
(15) Huang, W.; Hu, G. B.; Liang, W. B.; Wang, J. M.; Lu, M. L.; Yuan, R.; Xiao, D. R. Ruthenium(II) Complex-Grafted Hollow Hierarchical Metal-Organic Frameworks with Superior Electrochemiluminescence Performance for Sensitive Assay of Thrombin. *Anal. Chem.* **2021**, *93*, 6239−6245.
(16) Ma, D. X.; Li, B. Y.; Shi, Z. Multi-functional sites catalysts based on post-synthetic modification of metal-organic frameworks. *Chin. Chem. Lett.* **2018**, *29*, 827−830.
(17) Qi, H. L.; Zhang, C. X. Electrogenerated Chemiluminescence Biosensing. *Anal. Chem.* **2020**, *92*, 524−534.
(18) Fang, Q. C.; Lin, Z. H.; Lu, F. S.; Chen, Y. W.; Huang, X. C.; Gao, W. H. A sensitive electrochemiluminescence immunosensor for the detection of PSA based on CdWS nanocrystals and Ag^{+}@UIO-66-NH_2 as a novel coreaction accelerator. *Electrochim. Acta* **2019**, *302*, 207−215.
(19) Song, X. Z.; Zhao, L.; Luo, C. N.; Ren, X.; Yang, L.; Wei, Q. Peptide-Based Biosensor with a Luminescent Copper-Based Metal-Organic Framework as an Electrochemiluminescence Emitter for Trypsin Assay. *Anal. Chem.* **2021**, *93*, 9704−9710.
(20) Pu, G. Q.; Yang, Z. F.; Wu, Y. L.; Wang, Z.; Deng, Y.; Gao, Y. J.; Zhang, Z.; Lu, X. Q. Investigation into the Oxygen-Involved Electrochemiluminescence of Porphyrins and Its Regulation by Peripheral Substituents/Central Metals. *Anal. Chem.* **2019**, *91*, 2319−2328.
(21) Li, S. S.; Gao, Y. Q.; Li, N.; Ge, L.; Bu, X. H.; Feng, P. Y. Transition metal-based bimetallic MOFs and MOF-derived catalysts for electrochemical oxygen evolution reaction. *Energy Environ. Sci.* **2021**, *14*, 1897−1927.
(22) Liu, Y. T.; Lei, J. P.; Huang, Y.; Ju, H. X. "Off-On" Electrochemiluminescence System for Sensitive Detection of ATP via Target-Induced Structure Switching. *Anal. Chem.* **2014**, *86*, 8735−8741.
(23) Wu, P.; Hou, X. D.; Xu, J. J.; Chen, H. Y. Electrochemically Generated versus Photoexcited Luminescence from Semiconductor Nanomaterials: Bridging the Valley between Two Worlds. *Chem. Rev.* **2014**, *114*, 11027−11059.
(24) Reshetnyak, O.; Koval'chuk, E. A possible scheme of electrochemiluminescence generation on platinum cathodes in aqueous solutions of peroxydisulfates. *Electrochim. Acta* **1998**, *43*, 465−469.
(25) Zhao, B. L.; Luo, Y. L.; Qu, X. D.; Hu, Q.; Zou, J. H.; He, Y.; Liu, Z. B.; Zhang, Y. W.; Bao, Y.; Wang, W.; Niu, L. Graphite-like Carbon Nitride Nanotube for Electrochemiluminescence Featuring High Efficiency, High Stability, and Ultrasensitive Ion Detection Capability. *J. Phys. Chem. Lett.* **2021**, *12*, 11191−11198.
(26) Yadav, P. K.; Kumari, N.; Pachfule, P.; Banerjee, R.; Mishra, L. Metal Zn(II), Cd(II), 1,10-Phenanthroline Containing Coordination Polymers Constructed on the Skeleton of Polycarboxylates: Synthesis, Characterization, Microstructural, and CO_2 Gas Adsorption Studies. *Cryst. Growth Des.* **2012**, *12*, 5311−5319.
(27) Haldar, R.; Matsuda, R.; Kitagawa, S.; George, S. J.; Maji, T. K. Amine-Responsive Adaptable Nanospaces: Fluorescent Porous Coordination Polymer for Molecular Recognition. *Angew. Chem., Int. Ed.* **2014**, *53*, 11772−11777.
(28) Cui, Y. J.; Yue, Y. F.; Qian, G. D.; Chen, B. L. Luminescent Functional Metal-Organic Frameworks. *Chem. Rev.* **2012**, *112*, 1126−1162.
(29) Ren, X. Y.; Lu, L. H. Luminescent nanoscale metal-organic frameworks for chemical sensing. *Chin. Chem. Lett.* **2015**, *26*, 1439−1445.
(30) Xu, R. Y.; Wang, Y. F.; Duan, X. P.; Lu, K. D.; Micheroni, D.; Hu, A. G.; Lin, W. B. Nanoscale Metal-Organic Frameworks for Ratiometric Oxygen Sensing in Live Cells. *J. Am. Chem. Soc.* **2016**, *138*, 2158−2161.
(31) Wang, X. X.; Wang, X. Q.; Niu, X. Y.; Hu, T. P. Three novel metal-organic frameworks based on an unsymmetrical rigid carboxylate ligand for luminescence sensing of nitrobenzene derivatives and magnetic properties. *CrystEngComm* **2016**, *18*, 7471−7477.
(32) Kökçam-Demir, Ü.; Goldman, A.; Esrafili, L.; Gharib, M.; Morsali, A.; Weingart, O.; Janiak, C. Coordinatively unsaturated metal sites (open metal sites) in metal-organic frameworks: design and applications. *Chem. Soc. Rev.* **2020**, *49*, 2751−2798.
(33) Richter, M. M. Electrochemiluminescence (ECL). *Chem. Rev.* **2004**, *104*, 3003−3036.
(34) Wei, H.; Wang, E. Electrochemiluminescence of tris(2,2′-bipyridyl)ruthenium and its applications in bioanalysis: a review. *Luminescence* **2011**, *26*, 77−85.

https://doi.org/10.1021/acsomega.3c02559
ACS Omega 2023, 8, 43463−43473